NPS ARCHIVE
1964
BENNETT, C.

SOME NUMERICAL EXPERIMENTS WITH THE PRIMITIVE EQUATIONS OF MOTION

CHARLES L. BENNETT
and
LESLIE L. BRITTEN

DUDLEY KNOX LIBRARY
NAVAL POSTGRADUATE SCHOOL
MONTEREY CA 93943-5101

LIBRARY
U.S. NAVAL POSTGRADUATE SCHOOL
MONTEREY, CALIFORNIA

SOME NUMERICAL EXPERIMENTS WITH THE PRIMITIVE EQUATIONS OF MOTION

* * * * *

Charles L. Bennett

and

Leslie L. Britten

SOME NUMERICAL EXPERIMENTS WITH THE PRIMITIVE EQUATIONS OF MOTION

by

Charles L. Bennett
Captain, United States Air Force

and

Leslie L. Britten
CWO-3, United States Air Force

Submitted in partial fulfillment of
the requirements for the degree of

MASTER OF SCIENCE
IN
METEOROLOGY

United States Naval Postgraduate School
Monterey, California
1 9 6 4

APS Archive
1962
Barnett, C.

LIBRARY
U.S. NAVAL POSTGRADUATE SCHOOL
MONTEREY, CALIFORNIA

SOME NUMERICAL EXPERIMENTS WITH THE PRIMITIVE EQUATIONS OF MOTION

by

Charles L. Bennett

and

Leslie L. Britten

This work is accepted as fulfilling
the thesis requirements for the degree of
MASTER OF SCIENCE
IN
METEOROLOGY
from the
United States Naval Postgraduate School

ABSTRACT

A simple primitive-equation model for numerical prediction of wind fields and temperature fields at 800 and 400 mb is developed and programmed. Numerical experiments are conducted with this model in an effort to suppress the spurious instability encountered in solution of the primitive equations. The model proves to be very sensitive to spatial finite-differencing schemes. The schemes developed in this study tend to suppress the instability resulting from truncation and round-off error. Instability resulting from unrealistic boundary conditions for a limited forecast region is reduced by not allowing advection across the boundaries and appears to be controlled by the finite-differencing schemes used in this study.

The writers wish to express their appreciation to Professor George J. Haltiner of the U. S. Naval Postgraduate School for his guidance, contributions and encouragement in this work. Appreciation is also expressed to the personnel of the U. S. Navy Fleet Numerical Weather Facility for their cooperation during the preparation of this paper.

TABLE OF CONTENTS

TABLE OF SYMBOLS

π -- sea-level pressure

P_t -- pressure at the top of the atmosphere

σ -- $\frac{p-P_t}{\pi}$

$\dot{\sigma}$ -- time rate of change of σ

F -- horizontal frictional force per unit mass

ϕ -- geopotential

V -- horizontal wind vector

f -- coriolis parameter

u -- $\frac{dx}{dt}$

v -- $\frac{dy}{dt}$

$\hat{k}$ -- unit vector in the vertical

η -- $\frac{\partial v}{\partial x} - \frac{\partial u}{\partial y} + f$

F_x, F_y -- horizontal components of the frictional force per unit mass

C_p -- the coefficient of specific heat at constant pressure

R -- the gas constant for dry air

T -- the absolute temperature

d -- the grid-net spacing

τ -- vertical stress

p -- pressure

V -- magnitude of horizontal wind vector

θ -- potential temperature

1. Introduction.

It is generally recognized that solution of the primitive-equations offers the most general and logical approach to numerical prediction. Previous attempts at solution of the primitive equations by numerical methods have met with limited success. However, interest has recently been stimulated in the primitive equations by unpublished reports indicating that Arakawa [7] has succeeded in developing a stable solution. The purpose of this study is to develop and program a simple 3-level primitive equation model and perform some numerical experiments. The main effort in these experiments is devoted to the suppression of spurious instability encountered in numerical solution of the primitive equations. It is hoped that this instability can be suppressed by a finite-differencing scheme that will in the mean conserve the sum of potential and kinetic energies.

2. The Model

Phillips [1] describes a coordinate system where the vertical coordinate p in the x, y, p, t-system is replaced by an independent variable σ, where $\sigma = \frac{p-P_t}{\pi}$. The following relation then holds, where ξ can be x, y, or t:

$$\left(\frac{\partial}{\partial \xi}\right)_p = \frac{\partial}{\partial \xi} - \frac{\sigma}{\pi}\frac{\partial \pi}{\partial \xi}\frac{\partial}{\partial \sigma} . \qquad (1)$$

The subscript p denotes derivatives taken along a constant pressure surface. The variable σ ranges monotonically from zero at the top of the atmosphere to unity at the ground.

If the above coordinate system is utilized the horizontal equation of motion becomes

$$\frac{\partial \mathbf{V}}{\partial t} + (\mathbf{V}\cdot\nabla)\mathbf{V} + \dot{\sigma}\frac{\partial \mathbf{V}}{\partial \sigma} + \nabla\phi - \frac{\sigma}{\pi}\frac{\partial \phi}{\partial \sigma}\nabla\pi + \mathbf{F} + f\hat{k}\times\mathbf{V} = 0. \qquad (2)$$

In this study it is assumed that the top of the atmosphere P_t is at 200 mb. The atmosphere is divided vertically by five levels as follows:

$\sigma_0 = 0$	p=200 mb
$\sigma_1 = 1/4$	p=400 mb
$\sigma_2 = 1/2$	p=600 mb
$\sigma_3 = 3/4$	p=800 mb
$\sigma_4 = 1$	SFC

For this model $\dot{\nabla}_1$, and $\dot{\nabla}_3$ will be approximated as follows:

$$\dot{\nabla}_1 \doteq \frac{\dot{\nabla}_0 + \dot{\nabla}_2}{2}, \quad \dot{\nabla}_3 \doteq \frac{\dot{\nabla}_4 + \dot{\nabla}_2}{2}. \tag{3}$$

Vertical velocities are identically zero at the top and bottom of the atmosphere ($\dot{\nabla}_0=0, \dot{\nabla}_4=0$), reducing $\dot{\nabla}_1$ and $\dot{\nabla}_3$ to

$$\dot{\nabla}_1 = \dot{\nabla}_3 \doteq \frac{\dot{\nabla}_2}{2}.$$

If the preceding simplifications are utilized and equation (2) is applied at the ∇_1 and ∇_3 levels, the following equations ensue

$$\frac{\partial \mathbb{V}_1}{\partial t} + (\mathbb{V}_1 \cdot \nabla)\mathbb{V}_1 + \frac{\dot{\nabla}_2}{2\Delta\nabla}(\mathbb{V}_3 - \mathbb{V}_1) + \nabla\phi_1 -$$

$$\frac{\nabla_1}{\pi}\frac{\partial \phi_1}{\partial \nabla}\nabla\pi + \mathbb{F}_1 + f\hat{k}\times\mathbb{V}_1 = 0 \tag{4}$$

$$\frac{\partial \mathbb{V}_3}{\partial t} + (\mathbb{V}_3 \cdot \nabla)\mathbb{V}_3 + \frac{\dot{\nabla}_2}{2\Delta\nabla}(\mathbb{V}_3 - \mathbb{V}_1) + \nabla\phi_3 -$$

$$\frac{\nabla_3}{\pi}\frac{\partial \phi_3}{\partial \nabla}\nabla\pi + \mathbb{F}_3 + f\hat{k}\times\mathbb{V}_3 = 0. \tag{5}$$

It is assumed in (4) and (5) that

$$\frac{\partial \mathbb{V}_1}{\partial \nabla} = \frac{\partial \mathbb{V}_3}{\partial \nabla} = \frac{\partial \mathbb{V}_2}{\partial \nabla} = \frac{\mathbb{V}_3 - \mathbb{V}_1}{\Delta\nabla}.$$

Moreover the term $\nabla_1 \frac{\partial \phi_1}{\partial \nabla}$ in (4) may be replaced by

$$\nabla_1 \frac{\partial \phi_1}{\partial \nabla} = \left(\frac{\partial \phi \nabla}{\partial \nabla}\right)_1 - \phi_1 \frac{\partial \nabla_1}{\partial \nabla} .$$

Since $\nabla_0 = 0$ and $\frac{\partial \nabla_1}{\partial \nabla} = 1$,

$$\nabla_1 \frac{\partial \phi_1}{\partial \nabla} = \frac{\phi_2 \nabla_2}{\Delta \nabla} - \phi_1 ,$$

and equation (4) becomes

$$\frac{\partial \mathbb{V}_1}{\partial t} + (\mathbb{V}_1 \cdot \nabla)\mathbb{V}_1 + \frac{\dot{\nabla}_2}{2\Delta\nabla}(\mathbb{V}_3 - \mathbb{V}_1) + \nabla\phi_1 + \left(\phi_1 - \frac{\nabla_2 \phi_2}{\Delta \nabla}\right)\frac{1}{\pi}\nabla\pi + \mathbb{F}_1 + \hat{k} \times f \mathbb{V}_1 = 0. \qquad (6)$$

Similiarly at the ∇_3 level

$$\nabla_3 \frac{\partial \phi_3}{\partial \nabla} = \frac{\nabla_2 \phi_2 - \nabla_4 \phi_4}{\Delta \nabla} - \phi_3$$

and equation (5) becomes

$$\frac{\partial \mathbb{V}_3}{\partial t} + (\mathbb{V}_3 \cdot \nabla)\mathbb{V}_3 + \frac{\dot{\nabla}_2}{2\Delta\nabla}(\mathbb{V}_3 - \mathbb{V}_1) + \nabla\phi_3 + \left[\phi_3 - \frac{1}{\Delta\nabla}(\nabla_4\phi_4 - \nabla_2\phi_2)\right]\frac{1}{\pi}\nabla\pi + \mathbb{F}_3 + \hat{k} \times f \mathbb{V}_3 = 0. \qquad (7)$$

Equations (6) and (7) may also be expressed in component form as follows:

$$\frac{\partial u_1}{\partial t} = -\left[u_1\frac{\partial u_1}{\partial x} + v_1\frac{\partial v_1}{\partial x} - \eta_1 v_1\right] - \frac{\dot{\nabla}_2}{2\Delta\nabla}(u_3 - u_1) -$$

$$\frac{\partial \Phi_1}{\partial x} - \left(\Phi_1 - \frac{\nabla_2\Phi_2}{\Delta\nabla}\right)\frac{1}{\pi}\frac{\partial \pi}{\partial x} + F_{1x} \qquad (8)$$

$$\frac{\partial v}{\partial t} = -\left[u_1\frac{\partial u_1}{\partial y} + v_1\frac{\partial v_1}{\partial y} + \eta_1 u_1\right] - \frac{\dot{\nabla}_2}{2\Delta\nabla}(v_3 - v_1) - \frac{\partial \Phi_1}{\partial y} -$$

$$\left(\Phi_1 - \frac{\nabla_2\Phi_2}{\Delta\nabla}\right)\frac{1}{\pi}\frac{\partial \pi}{\partial y} + F_{1y} \qquad (9)$$

$$\frac{\partial u_3}{\partial t} = -\left[u_3\frac{\partial u_3}{\partial x} + v_3\frac{\partial v_3}{\partial x} - \eta_3 v_3\right] - \frac{\dot{\nabla}_2}{2\Delta\nabla}(u_3 - u_1) - \frac{\partial \Phi_3}{\partial x} -$$

$$\left[\Phi_3 - \frac{1}{\Delta\nabla}\left(\nabla_4\Phi_4 - \nabla_2\Phi_2\right)\right]\frac{1}{\pi}\frac{\partial \pi}{\partial x} - F_{3x} \qquad (10)$$

$$\frac{\partial v_3}{\partial t} = -\left[u_3\frac{\partial u_3}{\partial y} + v_3\frac{\partial v_3}{\partial y} + \eta_3 u_3\right] - \frac{\dot{\nabla}_2}{2\Delta\nabla}(v_3 - v_1) - \frac{\partial \Phi_3}{\partial y} -$$

$$\left[\Phi_3 - \frac{1}{\Delta\nabla}\left(\nabla_4\Phi_4 - \nabla_2\Phi_2\right)\right]\frac{1}{\pi}\frac{\partial \pi}{\partial y} - F_{3y} \qquad (11)$$

The equation of continuity expressed in ∇ coordinates becomes

$$\frac{\partial \pi}{\partial t} + \nabla\cdot(\pi V) + \frac{\partial}{\partial \nabla}(\pi\dot{\nabla}) = 0 \ . \qquad (12)$$

This equation can be combined with the thermodynamic equation

$$\frac{\partial \theta}{\partial t} + V\cdot\nabla\theta + \dot{\nabla}\frac{\partial \theta}{\partial \nabla} = 0 \qquad (13)$$

to yield

$$\frac{\partial(\Pi\Theta)}{\partial t} + \nabla\cdot(\Pi\Theta\mathbb{V}) + \frac{\partial}{\partial\nabla}(\Pi\Theta\dot{\nabla}) = 0. \tag{14}$$

Taking the dot product between $\Pi\mathbb{V}$ and equation (2) leads to

$$\frac{\Pi}{2}\frac{\partial V^2}{\partial t} + \frac{\Pi}{2}\mathbb{V}\cdot\nabla V^2 + \frac{\Pi}{2}\dot{\nabla}\frac{\partial V^2}{\partial\nabla} +$$

$$\Pi\mathbb{V}\cdot\nabla\phi - \nabla\mathbb{V}\cdot\nabla\Pi = 0. \tag{15}$$

Multiplying (12) by ϕ and utilizing the relationship

$$\Pi\mathbb{V}\cdot\nabla\phi = \nabla\cdot(\Pi\mathbb{V}\phi) - \phi\nabla\cdot(\Pi\mathbb{V})$$

results in

$$\Pi\mathbb{V}\cdot\nabla\phi = \nabla\cdot(\Pi\mathbb{V}\phi) + \phi\frac{\partial\Pi}{\partial t} + \phi\frac{\partial(\Pi\dot{\nabla})}{\partial\nabla}.$$

Substituting the identities

$$\phi\frac{\partial\Pi}{\partial t} = \left(\frac{\partial(\phi\nabla)}{\partial\nabla} - \nabla\frac{\partial\phi}{\partial\nabla}\right)\frac{\partial\Pi}{\partial t}$$

and

$$\phi\frac{\partial}{\partial\nabla}(\Pi\dot{\nabla}) = \frac{\partial(\phi\dot{\nabla}\Pi)}{\partial\nabla} - \Pi\dot{\nabla}\frac{\partial\phi}{\partial\nabla}.$$

into (15) and adding (15) to (12) yields a kinetic energy equation of the form

$$\frac{\partial}{\partial t}\left(\frac{\pi}{2}V^2\right)+\nabla\cdot\left(\frac{\pi}{2}V^2\mathbf{V}+\pi\phi\mathbf{V}\right)+\frac{\partial}{\partial\sigma}\left(\frac{\pi}{2}V^2\dot{\sigma}+\pi\phi\dot{\sigma}\right)+$$

$$\frac{\partial}{\partial\sigma}(\phi\sigma)\frac{\partial\pi}{\partial t}-\left(\sigma\frac{\partial\pi}{\partial t}+\sigma\mathbf{V}\cdot\nabla\pi+\pi\dot{\sigma}\right)\frac{\partial\phi}{\partial\sigma}=0. \qquad (16)$$

The first law of thermodynamics applied to adiabatic conditions is

$$C_p\frac{dT}{dt}-\alpha\frac{dp}{dt}=0 \quad .$$

Substituting $p=\pi\sigma+P_t$ and expanding the total derivatives into Eulerian form for σ coordinates leads to

$$\frac{\partial}{\partial t}(C_pT)+\mathbf{V}\cdot\nabla(C_pT)+\dot{\sigma}\frac{\partial(C_pT)}{\partial\sigma}-\alpha\left[\frac{\partial(\pi\sigma)}{\partial t}+\right.$$

$$\left.\mathbf{V}\cdot\nabla(\pi\sigma)+\dot{\sigma}\frac{\partial(\pi\sigma)}{\partial\sigma}\right]=0.$$

Multiplying this equation by π and equation (12) by C_pT, then adding the resulting equations gives the potential energy equation

$$\frac{\partial}{\partial t}(\pi C_pT)+\nabla\cdot(\pi C_pT\mathbf{V})+\frac{\partial}{\partial\sigma}(\pi C_pT\dot{\sigma})-\pi\alpha\left[\frac{\partial(\pi\sigma)}{\partial t}+\right.$$

$$\left.\mathbf{V}\cdot\nabla(\pi\sigma)+\dot{\sigma}\frac{\partial(\pi\sigma)}{\partial\sigma}\right]=0. \qquad (17)$$

Combining equations (16) and (17) gives

$$\frac{\partial}{\partial t}\left(\pi c_p T + \frac{\Pi}{2} V^2\right) + \nabla\cdot\left(\pi c_p T \mathbf{V} + \frac{\Pi}{2} V^2 \mathbf{V} + \pi\phi\mathbf{V}\right) +$$

$$\frac{\partial}{\partial \sigma}\left(\pi c_p T\dot{\sigma} + \frac{\Pi}{2} V^2\dot{\sigma} + \pi\phi\dot{\sigma}\right) + \frac{\partial \Pi}{\partial t}\frac{\partial(\phi\sigma)}{\partial \sigma} = 0. \qquad (18)$$

Thompson [4] outlines the following three main aspects to be considered in solving the primitive equations: formulation of boundary conditions, formulation of initial conditions and numerical integration of finite difference equations.

The method of numerical integration utilized in this study will be the method of repeated time extrapolation outlined by Thompson and shown to be computationally stable for a simple linear model with a grid interval the size of the one used in this study if the time interval is about 10 min. or less. This method employs a centered difference of the form

$$\phi_{t=m+1} = \phi_{t=m-1} + \left(\frac{\partial \phi}{\partial t}\right)_{t=m} 2\Delta t.$$

Initial conditions for solution of the primitive equations present a real problem. For meteorologically significant large-scale motion there is a near balance between the coriolis and pressure forces. This means the resultant acceleration is an order of magnitude smaller than either of these two forces. Small errors in the

measurement of initial wind and pressure fields may lead to intense divergence fields which, in turn, give large pressure changes, thus creating rapid accelerations. These spurious accelerations create fictitious gravity waves. To exclude these waves initially in this study, a form of non-divergent initial winds is used. However, this does not necessarily exclude gravity waves for all time.

The forecast region used in this study covers the major portion of the Northern Hemisphere. Boundary conditions for a limited region such as this are difficult to define since the proper type of boundary conditions depends on the mathematical character of the primitive equations, which have a shifting dual nature, sometimes elliptic and sometimes hyperbolic. In this paper all parameters are assumed constant with respect to time on the boundaries. It is recognized that this assumption may lead to the existence of spurious development near the boundaries; however, it is felt that if the spatial finite-difference schemes are such that in the mean potential and kinetic energies are conserved, any boundary instability will tend to be averaged out over the forecast region. This averaging process will also tend to suppress spurious gravity waves resulting from truncation and round-off errors.

It has been shown by application (see, for example, Haltiner [6]) of Gauss' equation that when an equation

of the same type as (18) is integrated over a closed volume the local time change of the sum of kinetic and potential energy vanishes. It follows that any finite-difference scheme should in the mean conserve the sum of the potential and kinetic energies. Specifically, this consistency should be achieved separately with respect to both vertical and horizontal differencing.

The vertical consistency is developed as follows. First equation (15) is applied at the ∇_1 level. The vertical differencing is then performed, leading to

$$\frac{\partial}{\partial t}\left(\frac{\pi}{2} V_1^2\right) - \nabla\cdot\left(\frac{\pi}{2} V_1^2 V_1 + \pi V_1 \phi_1\right) + \frac{1}{\Delta\nabla}\left(\frac{\pi}{2} V_1 V_3 + \pi\phi_2\right)\dot{\nabla}_2 + \frac{\phi_2 \nabla_2}{\Delta\nabla}\frac{\partial \pi}{\partial t} + \left[\left(\phi_1 - \frac{\phi_2 \nabla_2}{\Delta\nabla}\right)\left(\frac{\partial \pi}{\partial t} + V_1\cdot\nabla\pi\right) + \frac{1}{\Delta\nabla}(\phi_1 - \phi_2)\pi\dot{\nabla}\right] = 0, \tag{19}$$

since $\dot{\nabla}_0 = 0$, $\nabla_0 = 0$ and $V_2^2 \doteq V_1 V_3$. The derivative $\frac{\partial \phi}{\partial \nabla}$ is approximated by a one-sided difference. A similar application of equation (17) results in

$$\frac{\partial}{\partial t}(\pi C_p T_1) + \nabla\cdot(\pi C_p T_1 V_1) + \frac{1}{\Delta\nabla}(\dot{\nabla}\pi C_p T_2) - \frac{\pi\nabla_1}{\pi\nabla_1 + p_T} R T_1 \left(\frac{\partial \pi}{\partial t} + V_1\cdot\nabla\pi\right) - \frac{\dot{\nabla}\pi}{\Delta\nabla} C_p\left[T_2 - \frac{1}{2}\left(T_1 + \left(\frac{p_1}{p_3}\right)^{\kappa} T_3\right)\right] = 0. \tag{20}$$

Adding equations (19) and (20) and comparing the result with equation (18) leads to the conclusion that if the consistency discussed in the previous paragraph is to be maintained, certain terms of equation (19) must cancel corresponding terms of equation (20). This inference leads to the following equivalences:

$$\frac{\pi \sigma_1}{\pi \sigma_1 + p_T} R T_1 = \Phi_1 - \Phi_2 = C_p \left[T_2 - \frac{1}{2} \left(T_1 + \left(\frac{p_1}{p_3} \right)^{\kappa} T_3 \right) \right],$$

A similar procedure at the σ_3 level utilizing the identity

$$\sigma \left(\frac{\partial \Phi}{\partial \sigma} \right) = \frac{\partial (\sigma \Phi)}{\partial \sigma} - \Phi$$

leads to

$$\frac{\pi \sigma_3}{\pi \sigma_3 + p_T} R T_3 = \Phi_2 + \Phi_3 - 2\Phi_4$$

and

$$\Phi_2 - \Phi_3 = C_p \left[\tfrac{1}{2} \left(T_3 + \left(\frac{p_3}{p_1} \right)^{k} T_1 \right) - T_2 \right].$$

From the previous equations the following relationships can be obtained.

$$T_2 = \left(\frac{\tfrac{1}{2} + \pi \sigma_1 k}{\pi \sigma_1 + p_T} \right) T_1 + \frac{1}{2} \left(\frac{p_1}{p_3} \right)^{k} T_3.$$

Substituting $P_t = 200$ mb, $p_1 = 400$ mb, $p_3 = 800$ mb $k = 0.286 j/g^{\circ}k$, $\sigma_1 = \frac{1}{4}$ and $C_p = 1.003 j/g^{\circ}k$ in the previous system

of equations leads to

$$T_2 = .643\ T_1 + .410\ T_3 \tag{21}$$

$$\Phi_1 = \Phi_4 + .442\ RT_1 + .530\ RT_3 \tag{22}$$

$$\Phi_2 = -.058\ RT_1 + .530\ RT_3 \tag{23}$$

$$\Phi_3 = \Phi_4 + .058\ RT_1 + .22\ RT_3 \tag{24}$$

If these relationships between geopotential and temperature are maintained then the vertical differencing scheme will not violate the energy conservation equations.

With respect to simple derivatives of the form $\frac{\partial \Phi}{\partial \chi}$ involved in (15), the centered difference approximation

$$\left(\frac{\partial \Phi}{\partial \chi}\right)_i \doteq \frac{\Phi_{i+1} - \Phi_{i-1}}{2\Delta\chi}$$

will obviously vanish when summed over interior points of the grid and thus would in the mean conserve potential and kinetic energy. However this does not take care of the boundaries, nor terms which are not of the simple form shown above.

Since numerical integration is to be performed by repeated time extrapolation, the velocity tendencies (8) - (11) will have to be computed from Φ, T and $\dot{\nabla}_2$ after they have been extrapolated forward in time. This will require tendency equations for $\overline{\pi}$ and T since Φ values are expressed in terms of T through equations (22) - (24).

Integration of (12) leads to the approximate form

$$\frac{\partial \overline{\pi}}{\partial t} \doteq -\frac{1}{2} \nabla \cdot \left[\overline{\pi}(V_1 + V_3)\right]. \tag{25}$$

From (12)

$$\frac{\pi \dot{\nabla}_2}{\Delta \nabla} = -\frac{\partial \pi}{\partial t} - \nabla \cdot (\pi V_1)$$

substituting for $\frac{\partial \pi}{\partial t}$ from (25) gives

$$\dot{\nabla}_2 \doteq \frac{\Delta \nabla}{\pi} \left[\nabla \cdot (\pi V_2 - \pi V_1) \right] .$$

The relationship

$$-\pi \alpha = \frac{\partial \Phi}{\partial \nabla}$$

utilized in equation (17) yields for the ∇_1 level

$$\pi C_p \frac{\partial T_1}{\partial t} + C_p T_1 \left[\frac{\partial \pi}{\partial t} + \nabla \cdot (\pi V_1) \right] + C_p \pi V_1 \cdot \nabla T_1 +$$

$$\frac{\Phi_2 - \Phi_1}{\Delta \nabla} \left[\frac{\partial \pi}{\partial t} + V_1 \cdot \nabla \pi \right] + \frac{\dot{\nabla} \pi}{\Delta \nabla} (\Phi_2 - \Phi_1 + C_p T_2) = 0 . \qquad (26)$$

The bracketed terms of equation (26) may be replaced by the following relationship

$$\frac{\partial \pi}{\partial t} + \nabla \cdot (\pi V_1) = -\frac{\pi \dot{\nabla}_2}{\Delta \nabla} .$$

Dividing (26) by πC_p gives

$$\frac{\partial T_1}{\partial t} + V_1 \cdot \nabla T_1 + \frac{\dot{\nabla}_2}{\Delta \nabla} (T_2 - T_1) = 0 . \qquad (27)$$

A similar approach at the ∇_3 level will result in the following tendency equation

$$\frac{\partial T_3}{\partial t} + V_3 \cdot \nabla T_3 + \frac{\dot{\nabla}_2}{\Delta \nabla} \left[.68 T_3 - T_2 - .033 T_1 \right] = 0 \qquad (28)$$

based on equations (21) - (24) with ϕ_4 assumed zero.

These tendency equations complete the system required for repeated time extrapolation.

3. Numerical experiments and results.

1. Energy Considerations

In the basic model, the energy balance with respect to vertical differencing is maintained through the relationship between temperature and geopotential developed in Section 2. With respect to horizontal differencing, the problem may be considered in two parts,

A. internal energy balance,

B. boundary effects.

For the former problem, partial derivatives of a "closed" form, such as $\frac{\partial \mathcal{E}_a}{\partial x}$, can be maintained in balance through use of a simple central differencing scheme. As the computation proceeds across the grid, each term is added and subtracted once at each grid point, with no change in total energy. However, a few derivatives with variable coefficients must be evaluated in the horizontal acceleration equations, (8) through (11), and also in the temperature-change and stability-change equations. In these terms, of the form $v\frac{\partial \mathcal{E}_a}{\partial x}$, the coefficient varies as the grid is traversed, so that the weighting of the term at a specific grid point changes between addition and subtraction in central differencing. This can lead to a change in total energy across the field, with resultant build-up of instability.

The following approaches were tested on these "open"

forms:

a. Terms left in this form.

This lead to a comparatively short set of forms. For example, the bracketed portion of equation (8) was simplified to $\frac{v_1 \partial u_1}{\partial y} - \frac{u_1 \partial u_1}{\partial x} - v_1 f$. However, this form did not fulfill the requirements for energy balance, and the model became unstable in a very short time with overflow occuring in less than four hours.

b. Terms placed in a "closed" form as a sum of squares.

The bracketed form of equation (8) now become

$$v_1 \eta_1 - \tfrac{1}{2} \frac{\partial (u_1^2 + v_1^2)}{\partial x}.$$

This form was a distinct improvement on the "open" form; however, variable coefficients involved in η_1, were not affected. In any case, there was some instability and this model overflowed in about six hours.

c. Open form with multipliers replaced by average values.

In this model, the equations of the first approach were used, but a "central average" replaced the variable coefficient in each case. For example, $\frac{v \partial u}{\partial y}$ became, in finite difference notation:

$$\frac{(v_{(J+1)} + v_{(J-1)})}{2} \frac{(u_{(J+1)} - u_{(J-1)})}{2\Delta y}$$

This model gave the best results of the three, and was used for the remaining experiments.

The problem of boundary effects proved much more difficult. Due to computer storage limitations, this model

was programmed using an octagonal grid whose southern boundaries are as much as 18° from the equator. Advection at these boundaries leads to major problems.

The following boundary forms were tested:

a. All time derivatives set equal to zero along the boundaries. Since the boundary values were held constant, while values at adjacent points were allowed to vary, large gradients resulted, giving large-amplitude gravity waves which moved inward from all sides at high speed. (See Fig. 1)

b. Boundary values averaged at short time intervals.

Several smoothing techniques were tried which involved only the outside three grid points. Since a gravity wave cannot cover the distance between two grid points in less than one hour of forecast time, this averaging was carried out once each hour. The most successful technique involved placing an average of the three outer points at the next-to-edge point, then averaging this value with that at the outside point and placing the result at the outside point. For example;

(Boundary)	A	B	C
becomes	$\frac{A+(A+B+C)/3}{2}$	$(A+B+C)/3$	C

This method restricted the instability due to boundary effects to the outer two grid points; however, in spite of the heavy averaging, large differences developed between the outer three grid points after about five hours fore-

cast time.

c. All horizontal velocities set equal to zero along the boundaries.

Since the instability developed along the boundaries can be traced to energy advected into or out of the forecast area, zeroing the horizontal winds at the boundaries, thereby zeroing the advection, should solve the problem. In practice, it was found that zeroing the horizontal wind components at both forecast levels at the outer two grid points was effective in controlling boundary-produced gravity waves. Surprisingly, this did not lead to instability in the wind-component fields themselves in this model. This method of boundary condition control was used throughout the remaining experiments.

2. Friction Terms

Two friction terms were developed for use with the horizontal acceleration equations (8) through (11). For horizontal friction, a simple Laplacian multiplied by $10^5 cm^2/sec$ was subtracted at each time step. For vertical friction, the terms developed by Smagorinsky [5] were used, with an average skin friction coefficient of 2.2×10^{-3} after Cressman [3]. According to Smagorinsky, the vertical friction at any level may be computed from

$$vF_k = -g\frac{\partial \tau}{\partial p} = \frac{g}{\Delta p}(\tau_{K+1} - \tau_{K-1}).$$

Assuming $\tau_0 = 0$,

$$vF_1 = \frac{g\tau_2}{\Delta p} \quad ; \quad vF_3 = \frac{g}{\Delta p}(\tau_4 - \tau_2)$$

Vertical stress, τ, is taken as a function of the vertical wind shear, so that

$$\tau_4 = \left(\frac{K\rho V}{\epsilon}\right)_4 ,$$

or since K is proportional to the magnitude of the wind, $|V|_4$ and ϵ is a constant for any roughness length

$$\tau_4 = \left(\frac{\rho C_d}{2} |\underline{V}| \underline{V}\right)_4$$

$\frac{C_d}{2}$ depends on roughness length, and from Cressman's paper an average value of 2.2×10^{-3} was used. Level 4 was taken to be the top of the friction level for this term, with $|V|_4$ estimated as a fraction of the vectorially extrapolated wind by the equation

$$|V|_4^2 = 0.36\,(\,(1.192u_3 - 0.192u_1)^2 + (1.192v_3 - 0.192v_1)^2\,) .$$

For V_4 the cross isobar angle at level 4 was taken to be a function of latitude alone by the equation

$$\text{ctn}\delta = 1 - 10^2\sqrt{2f} \quad , \; f \text{ in sec}^{-1},$$

This gives a cross-isobar angle ranging from near zero at the pole to approximately 35° at the base of the grid (18N), which is in close agreement with average values. The magnitude of V_4 was obtained from the geostrophic approximation and the ϕ_4 field, which in turn was estimated by a simple extrapolation from ϕ_1 and ϕ_3 , namely

$$\phi_4 = 1.192\,\phi_3 - 0.192\,\phi_1 \; ,$$

For τ_2, the equation,

$$\tau_2 = -(\rho K)_2 \frac{g\rho_2}{\Delta p} (V_1 - V_3)$$

can be readily obtained from the basic τ equation. Here $g\rho_2/\Delta P = 1/\Delta z$, where z=5.236 km, the standard depth of the 800- to 400-mb layer. For $(\rho K)_2$, the Rossby and Montgomery estimate of 500 gm/m sec was used.

This series of equations was programmed and tested on the model. However, the terms involved were so small compared to the rest of the model, and the computations so time-consuming (approximately 50% increase in computing time), that time was not available for a complete evaluation.

3. Prognosis of Surface Pressure

The prognosis of surface pressure was one of the most difficult problems encountered because the surface pressure change of the basic model was apparently very sensitive to small errors in velocity aloft. In fact, the surface pressure field served as a diagnostic chart, since any instability was apparent there long before it appeared aloft.

Four different methods were tried for obtaining the prognostic surface pressure field:

a. Expansion of the basic equation (25).

The resulting pressure-change field was extremely sensitive to changes in velocity divergence at levels 1 and 3, and large pressure changes occurred in two to three hours.

b. Averaging around the grid point.

In this approach, the products of the pressure value and the sum of the wind components at levels one and three were differenced across the point being computed. In finite difference form,

$$\frac{\partial \pi}{\partial t} = -\frac{1}{2}\frac{m}{2d}\Big[\pi_{(i+1)}\left(u_{1(i+1)} + u_{3(i+1)}\right) - \pi_{(i-1)}\left(u_{1(i-1)} + u_{3(i-1)}\right) +$$

$$\pi_{(j+1)}\left(v_{1(j+1)} + v_{3(j+1)}\right) - \pi_{(j-1)}\left(v_{1(j-1)} + v_{3(j-1)}\right)\Big] .$$

This model was not quite as sensitive to divergence errors, but still gave unreasonable surface pressure changes over periods as short as 6 hours.

c. Computation of surface pressure directly from the ϕ fields.

In this case, the deviation of the surface pressure from standard was estimated at each time step from the deviation of the ϕ fields from standard at 800 and 400 mb and the hydrostatic equation; i.e., if ϕ'_{400} is defined as $\phi_{400} - \phi_{(STD)\,400}$, etc, then

$$\phi'_{1000} = \phi'_{800} - \frac{\partial \phi'}{\partial p}\Delta p \doteq \phi'_{800} - \frac{\phi'_{400} - \phi'_{800}}{2}$$

and if we let $\phi'_{1000} \doteq \phi'_{SFC}$, then from the hydrostatic equation, $\Delta p \doteq \rho_{SFC}\phi'_{1000}$ and $p = p_{std} + \Delta p$.

This model was programmed and computed. However, since the ϕ fields are based on temperature and the basic inputs to this model were the temperature patterns at 400 and 800 mb, the resultant surface pressure field lacked some of the usual detail.

4. Conclusions and suggestions for further study

In this series of experiments, three finite difference forms, three boundary forms, and three surface pressure forms were tested. It was found that this model is extremely sensitive to finite difference forms used and boundary conditions assumed. However, when a new form gave a closer approximation to energy balance, stability was improved in every case, with the improvement noted being in direct proportion to the approach to energy balance.

It is the opinion of the writers that a stable primitive-equation model of this type can be achieved, and will eventually become the standard form of numerical prognosis. However, faster computers with much larger storage capacity must be used to realize this goal. At least two more levels of temperature input are needed to delineate the geopotential fields clearly, and the grid should be expanded to cover at least a whole hemisphere to reduce boundary problems. Even with high speed magnetic drum storage, such a model would have a prohibitively long running time on a computer such as the CDC 1604; but it might be completely feasible on the next generation of computers.

For the present, further experiments with surface pressure forms are suggested, possibly using some simplified version of the equations currently under development by Arakawa [7]. Also, the friction terms could be

streamlined and tested, and a surface terrain term included. However, any major revision of this model will require the use of a larger, faster computer than any currently available.

BIBLIOGRAPHY

1. Phillips, N.A., A coordinate system having some special advantages for numerical forecasting, J. of Meteor., Vol. 14, No. 4, pp 184-185, April 1957.

2. Lorenz, E.N., Energy and numerical weather prediction, Tellus, Vol. 22, No. 4, pp 364-375, November 1960.

3. Cressman, G.P., Improved terrain effects in barotropic forecasts, J. of Meteor., Vol. 88, Nos 9-12, pp 327-342, September-December 1960.

4. Thompson, P.D., Numerical weather analysis and prediction, The MacMillan Company, New York, 1961.

5. Smagorinsky, J., General circulation experiments with the primitive equations, Monthly Weather Review, Vol. 91, No. 3, pp 99-164, March 1963.

6. Haltiner, G.J., Weather prognosis by dynamical methods, Unpublished departmental notes, U. S. Naval Postgraduate School, 1962.

7. Arakawa, A., Unpublished notes.

APPENDIX I

LIST OF FIGURES

Figure

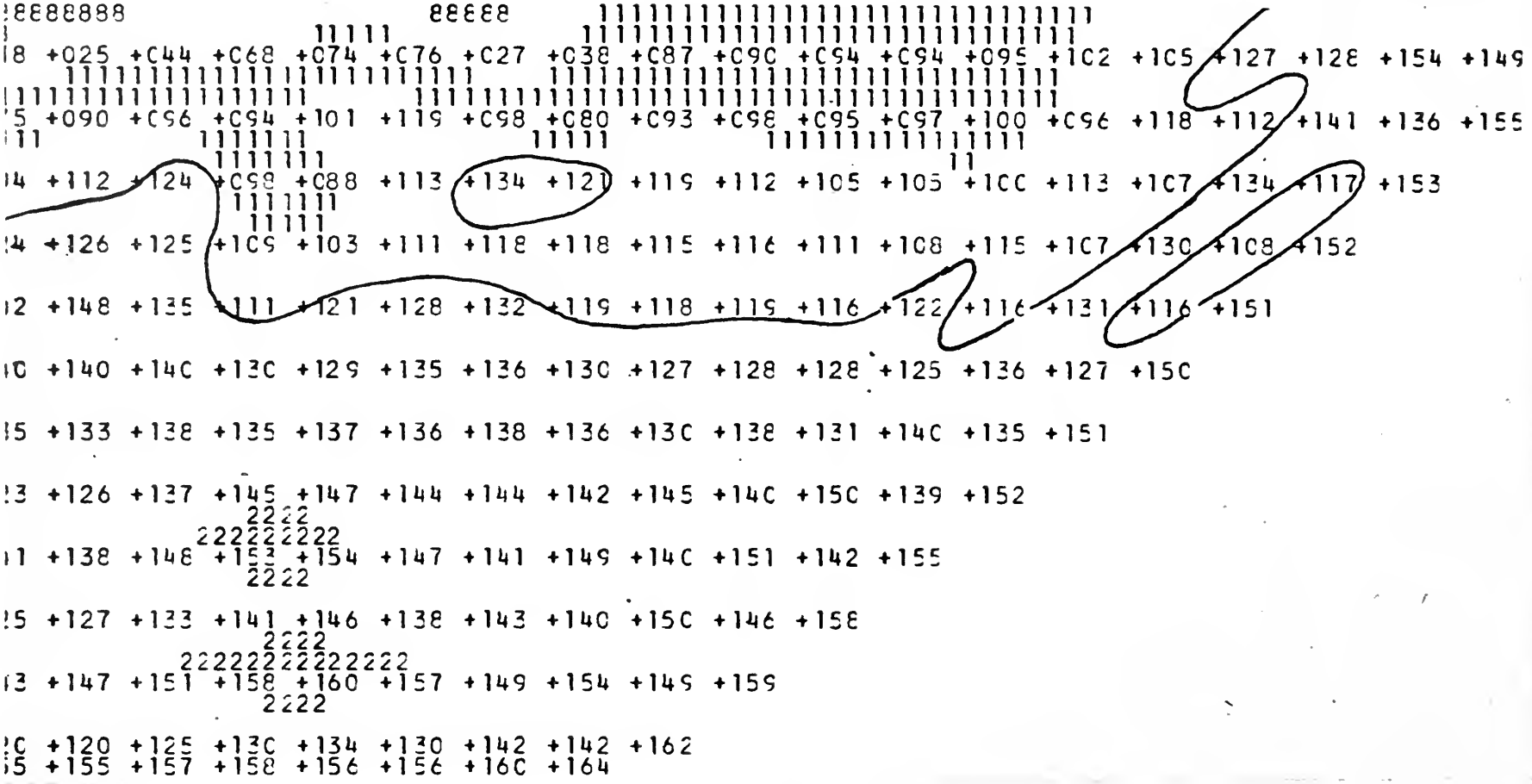

FIG.1 SECTION OF 6 HOUR 800 MB. TEMPERATURE PROGNOSIS

WITH NO BOUNDARY CORRECTION.

PLUS 12° ISOTHERM CONTOURED

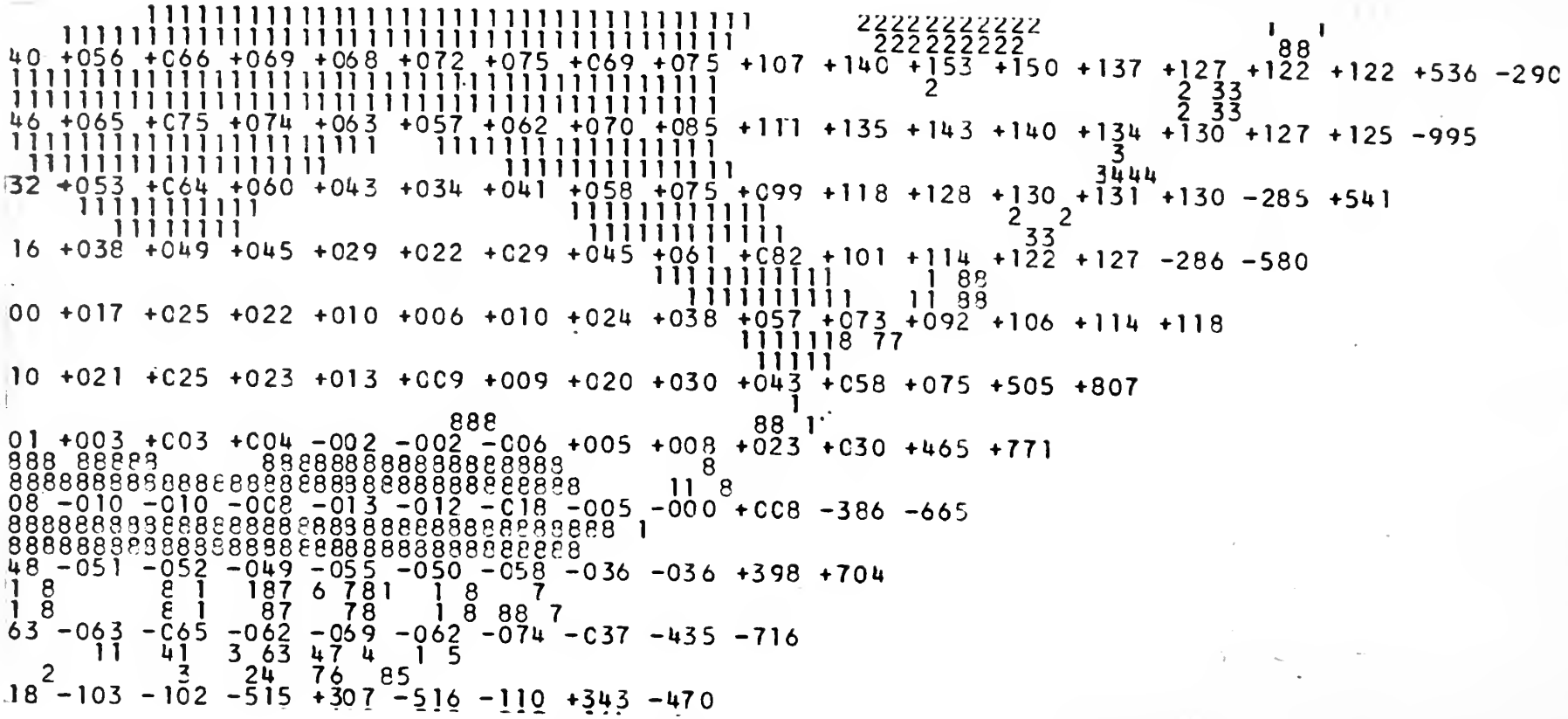

FIG.2 SECTION OF 12 HOUR 800 MB. TEMPERATURE PROGNOSIS

EDGE AVERAGED

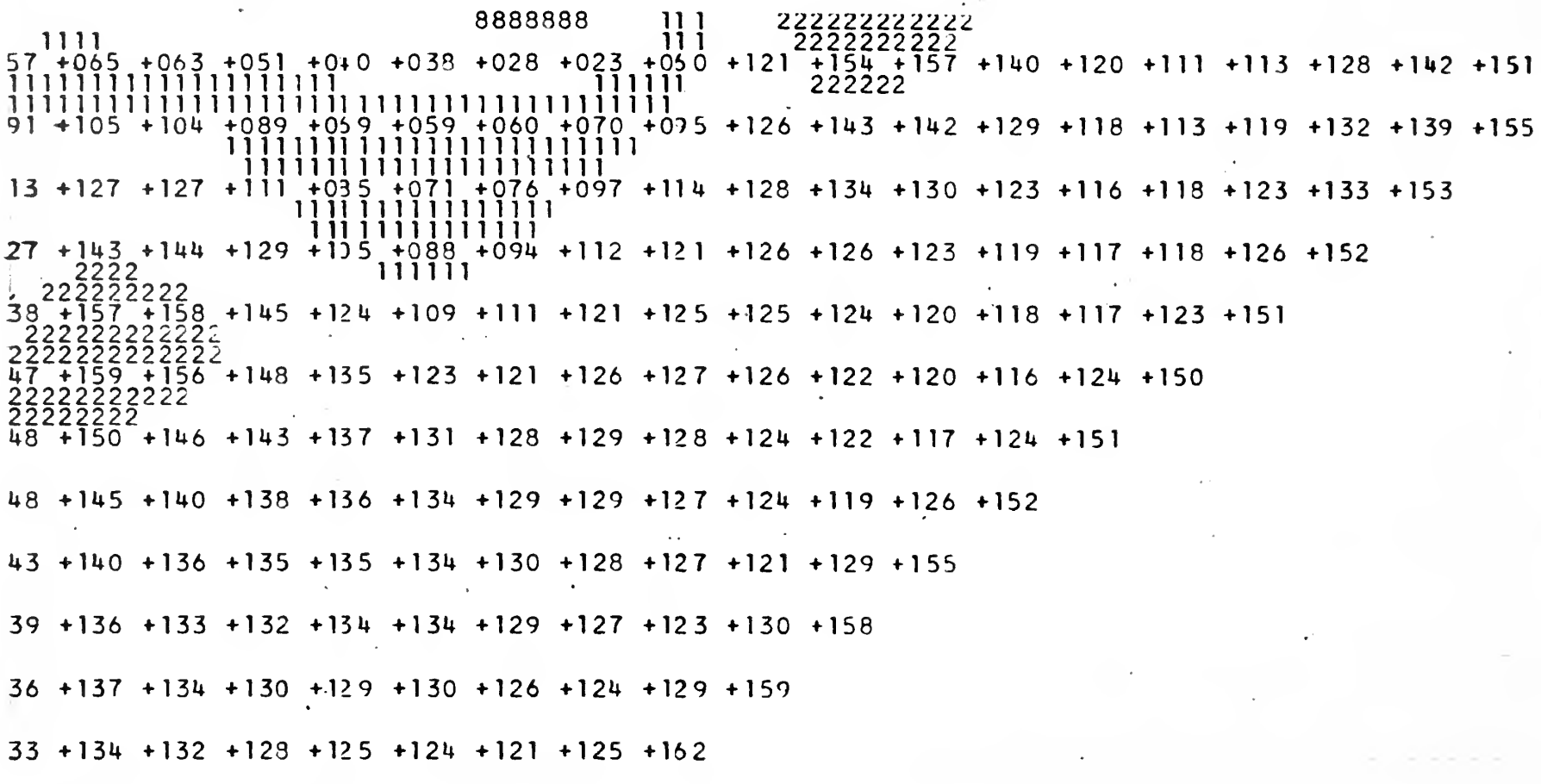

FIG.3 SECTION OF 18 HOUR 800 MB. TEMPERATURE PROGNOSIS

BOUNDARY ADVECTION ZEROED

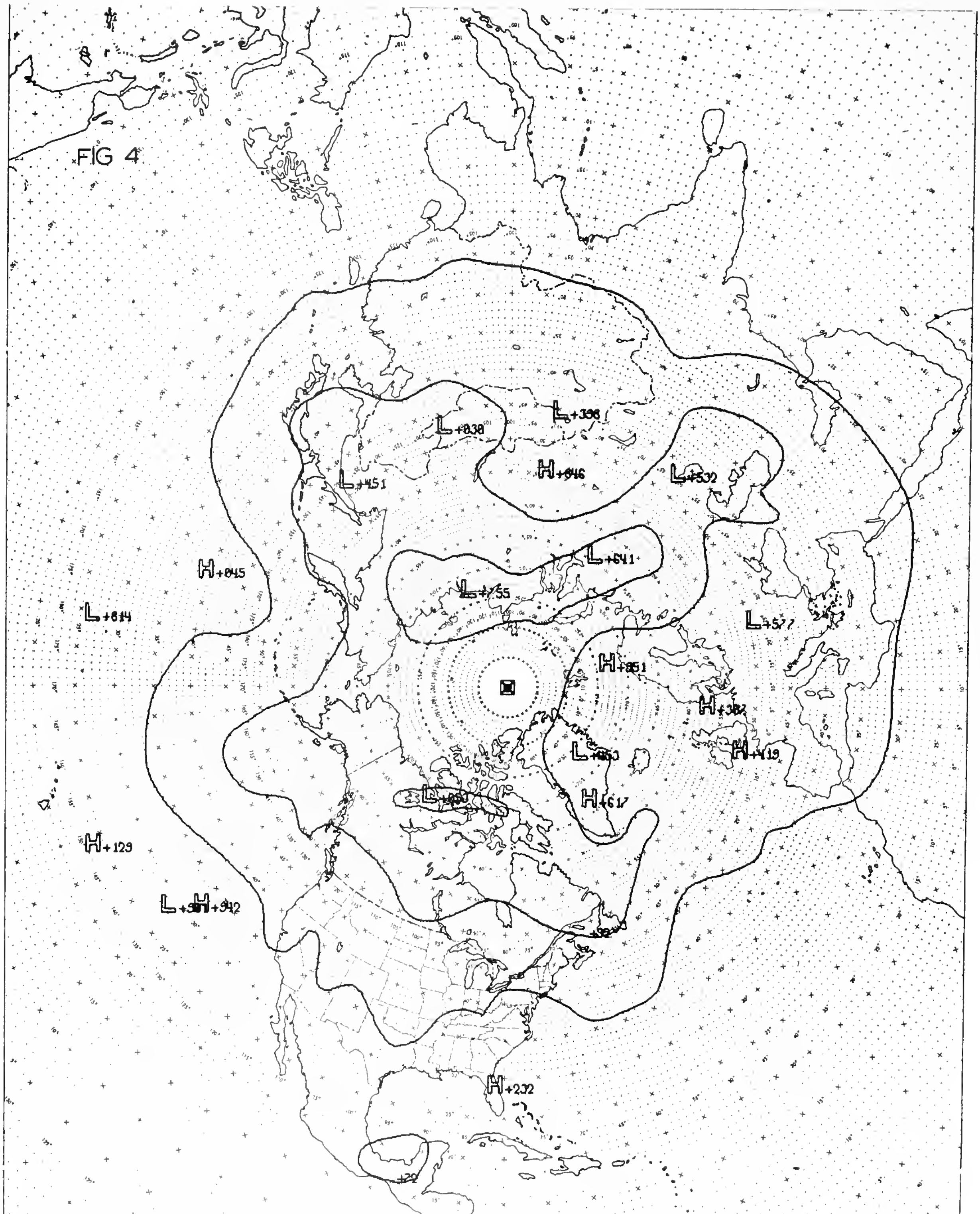
FIG 4
L+838
L+398
H+846
L+532
L+451
L+641
H+845
L+614
H+851
L+577
H+382
H+419
H+617
H+129
L+387 H+942
H+232
0 00Z 20 JAN 64 PH 800
PROJECTION: POLAR STEREOGRAPHIC—TRUE AT 60° NORTH LATITUDE
SCALE 1:60,000,000
FLEET NUMERICAL WEATHER FACILITY
MONTEREY, CALIFORNIA
CHART NO 6 B

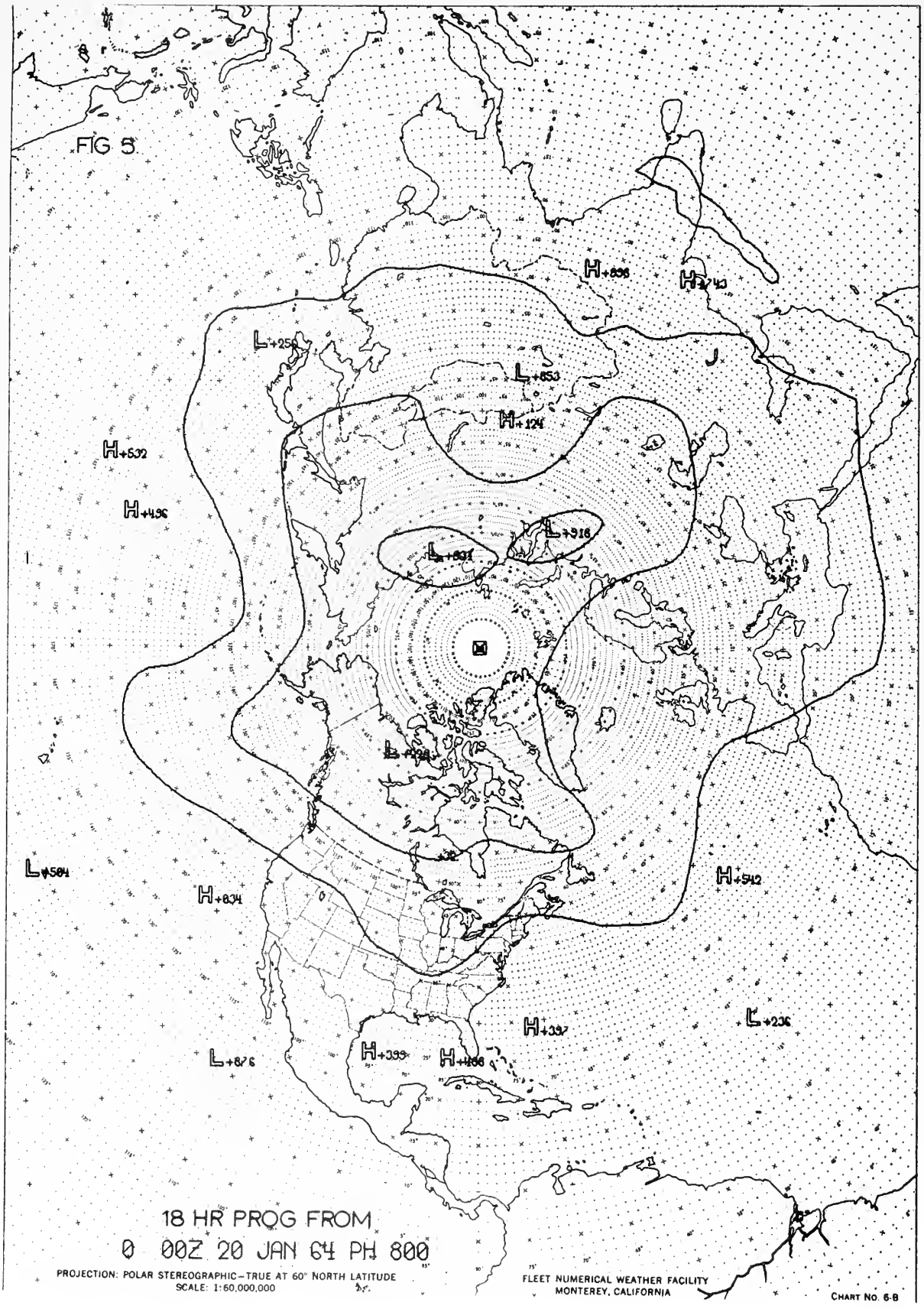
FIG 5
H+836
H+743
L+256
L+853
H+124
H+532
H+436
L+916
L+891
L+928
L+584
H+834
H+542
H+397
L+236
L+876
H+399
H+486
18 HR PROG FROM
0 00Z 20 JAN 64 PH 800
PROJECTION: POLAR STEREOGRAPHIC—TRUE AT 60° NORTH LATITUDE
SCALE: 1:60,000,000
FLEET NUMERICAL WEATHER FACILITY
MONTEREY, CALIFORNIA
CHART NO. 6-8

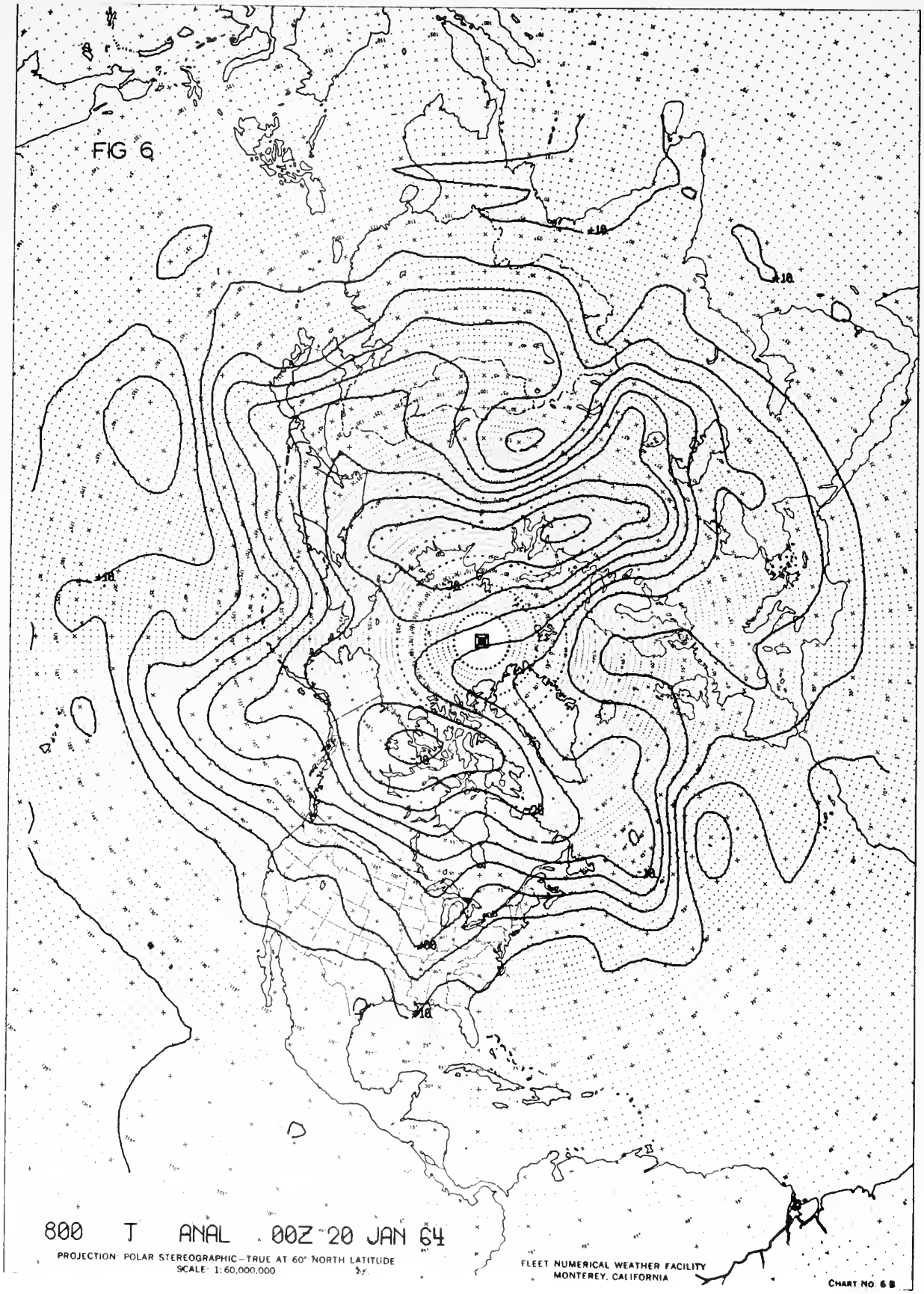
FIG 6
800 T ANAL 00Z 20 JAN 64
PROJECTION: POLAR STEREOGRAPHIC – TRUE AT 60° NORTH LATITUDE
SCALE: 1:60,000,000
FLEET NUMERICAL WEATHER FACILITY
MONTEREY, CALIFORNIA
CHART NO. 6 B

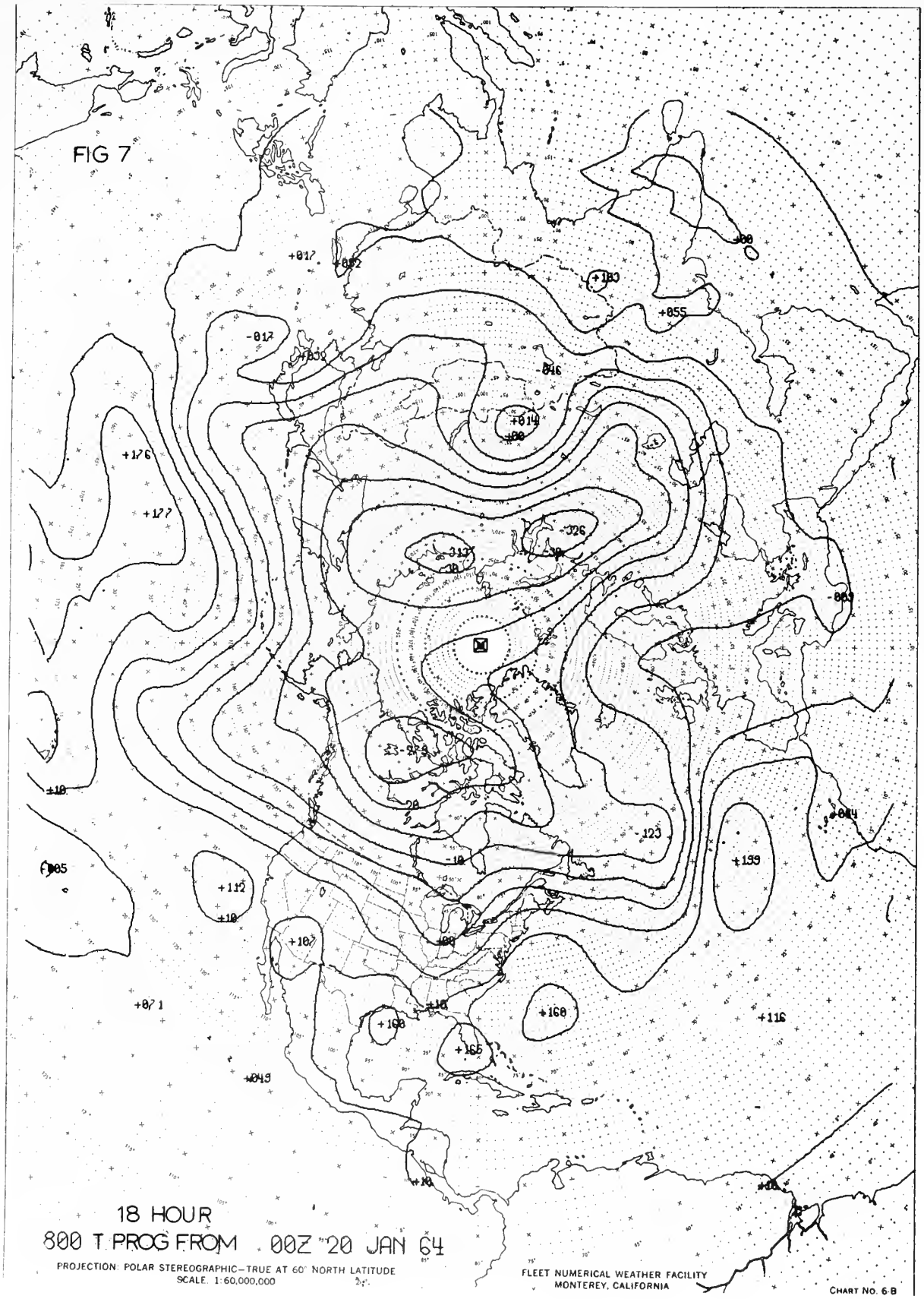
FIG 7
18 HOUR
800 T PROG FROM 00Z 20 JAN 64
PROJECTION: POLAR STEREOGRAPHIC – TRUE AT 60° NORTH LATITUDE
SCALE 1:60,000,000
FLEET NUMERICAL WEATHER FACILITY
MONTEREY, CALIFORNIA
CHART NO. 6-8

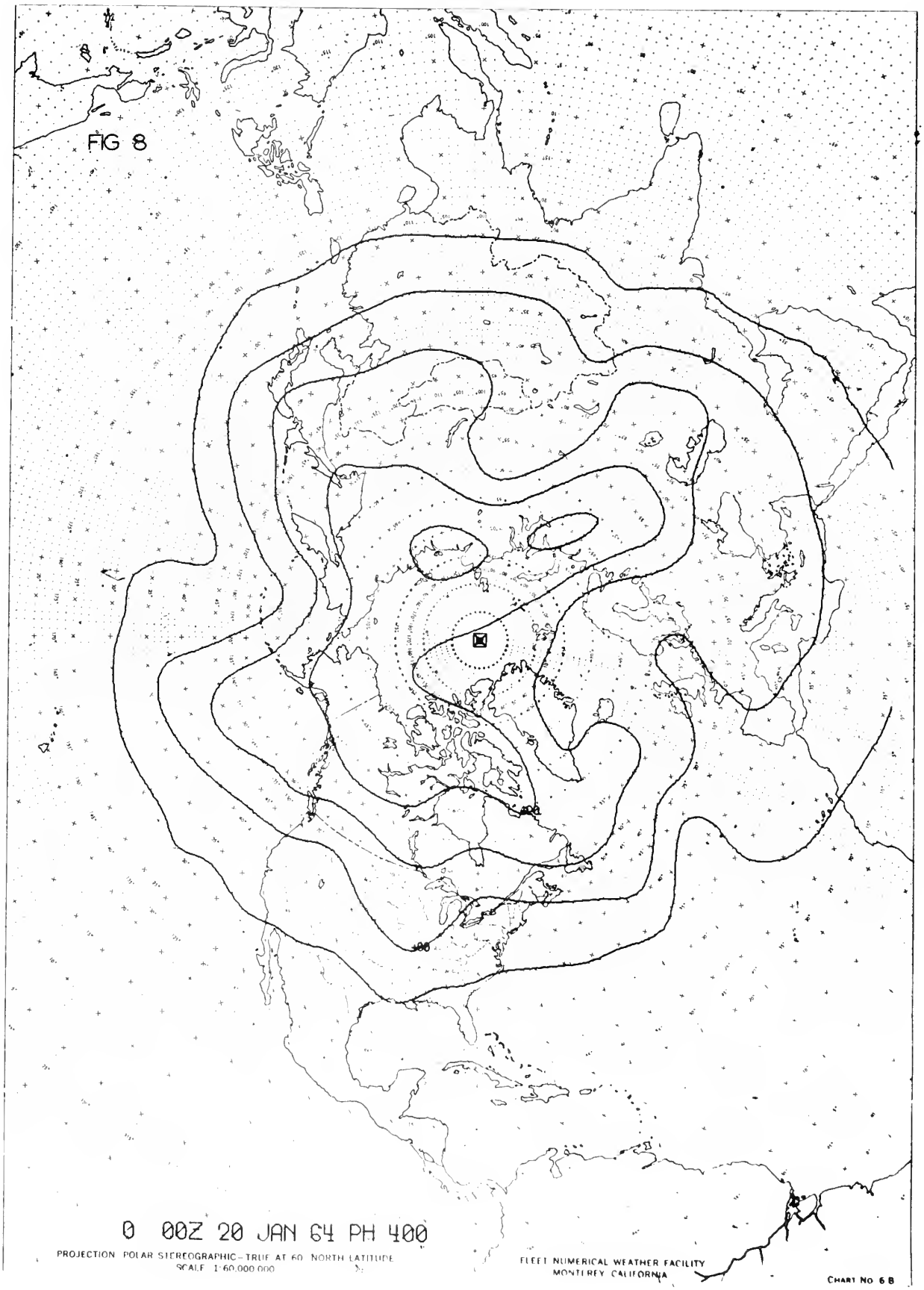
FIG 8
0 00Z 20 JAN 64 PH 400
PROJECTION POLAR STEREOGRAPHIC - TRUE AT 60 NORTH LATITUDE
SCALE 1:60,000,000
FLEET NUMERICAL WEATHER FACILITY
MONTEREY CALIFORNIA
CHART NO 6 B

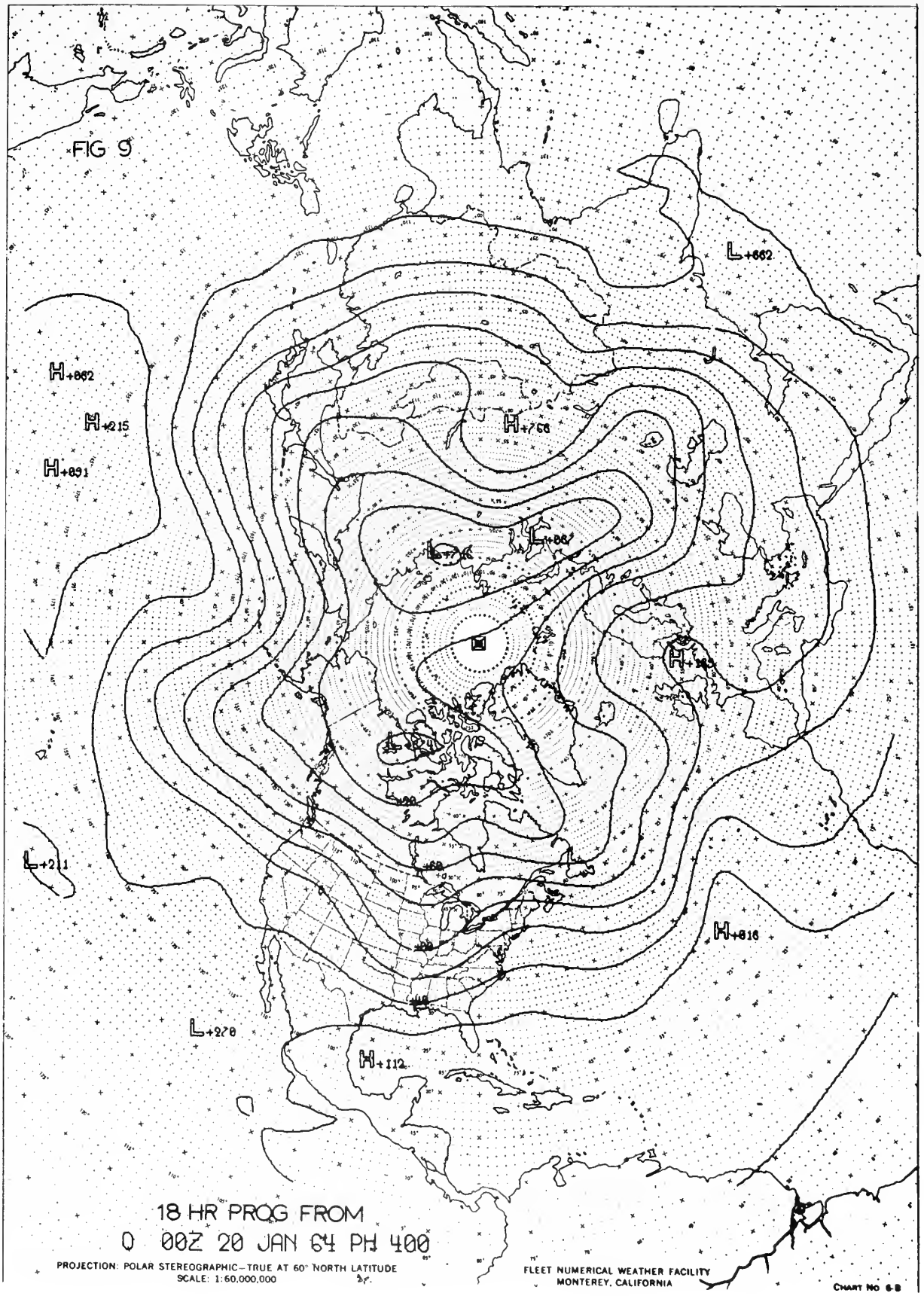
FIG 9
L+662
H+862
H+215
H+891
H+766
L+886
H+816
L+211
L+278
H+112
18 HR PROG FROM
0 00Z 20 JAN 64 PH 400
PROJECTION: POLAR STEREOGRAPHIC – TRUE AT 60° NORTH LATITUDE
SCALE: 1:60,000,000
FLEET NUMERICAL WEATHER FACILITY
MONTEREY, CALIFORNIA
CHART NO. 6-B

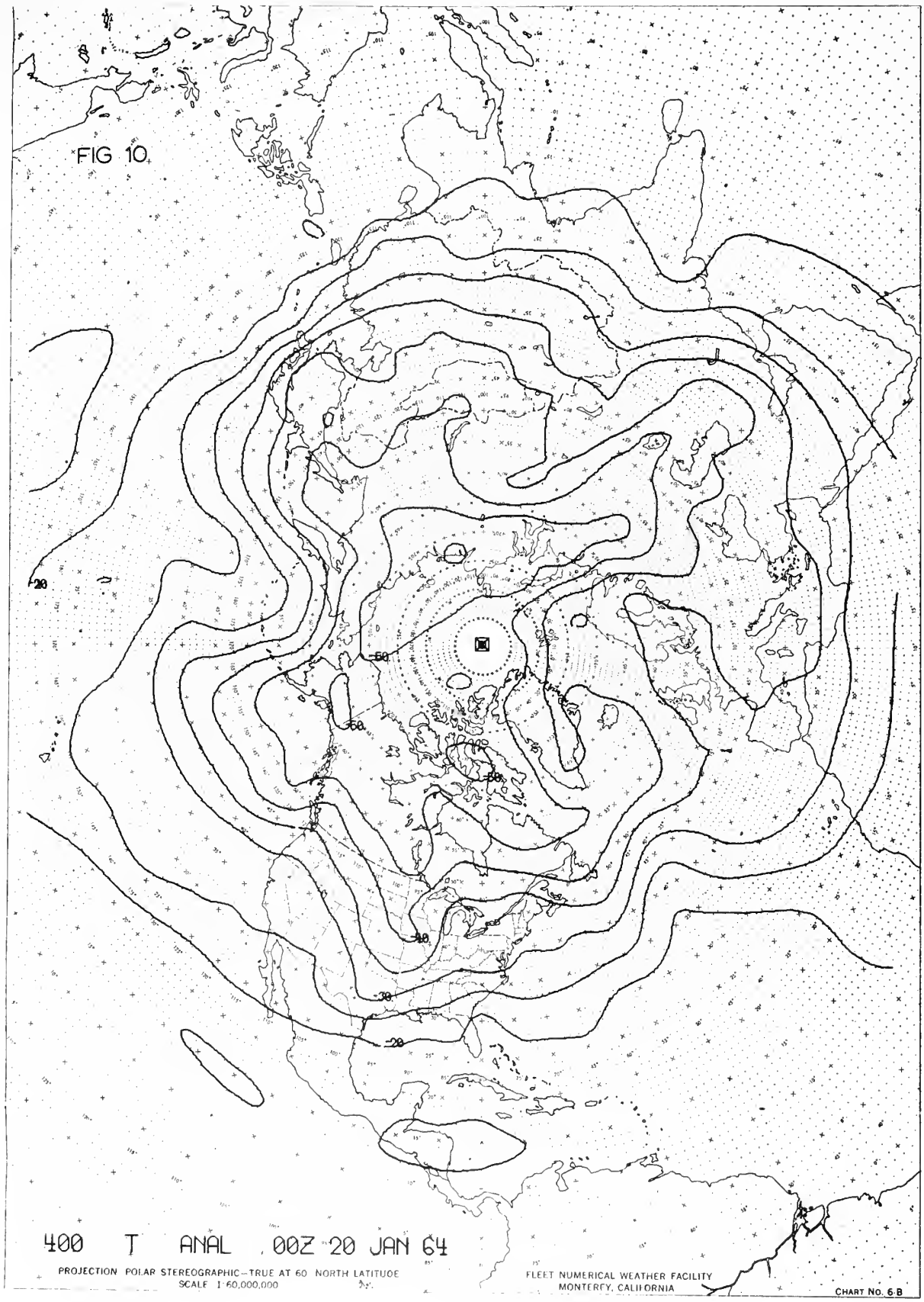
FIG 10
-20
-50
-60
-50
-40
-30
-20
400 T ANAL 00Z 20 JAN 64
PROJECTION POLAR STEREOGRAPHIC—TRUE AT 60 NORTH LATITUDE
SCALE 1:60,000,000
FLEET NUMERICAL WEATHER FACILITY
MONTEREY, CALIFORNIA
CHART NO. 6-B

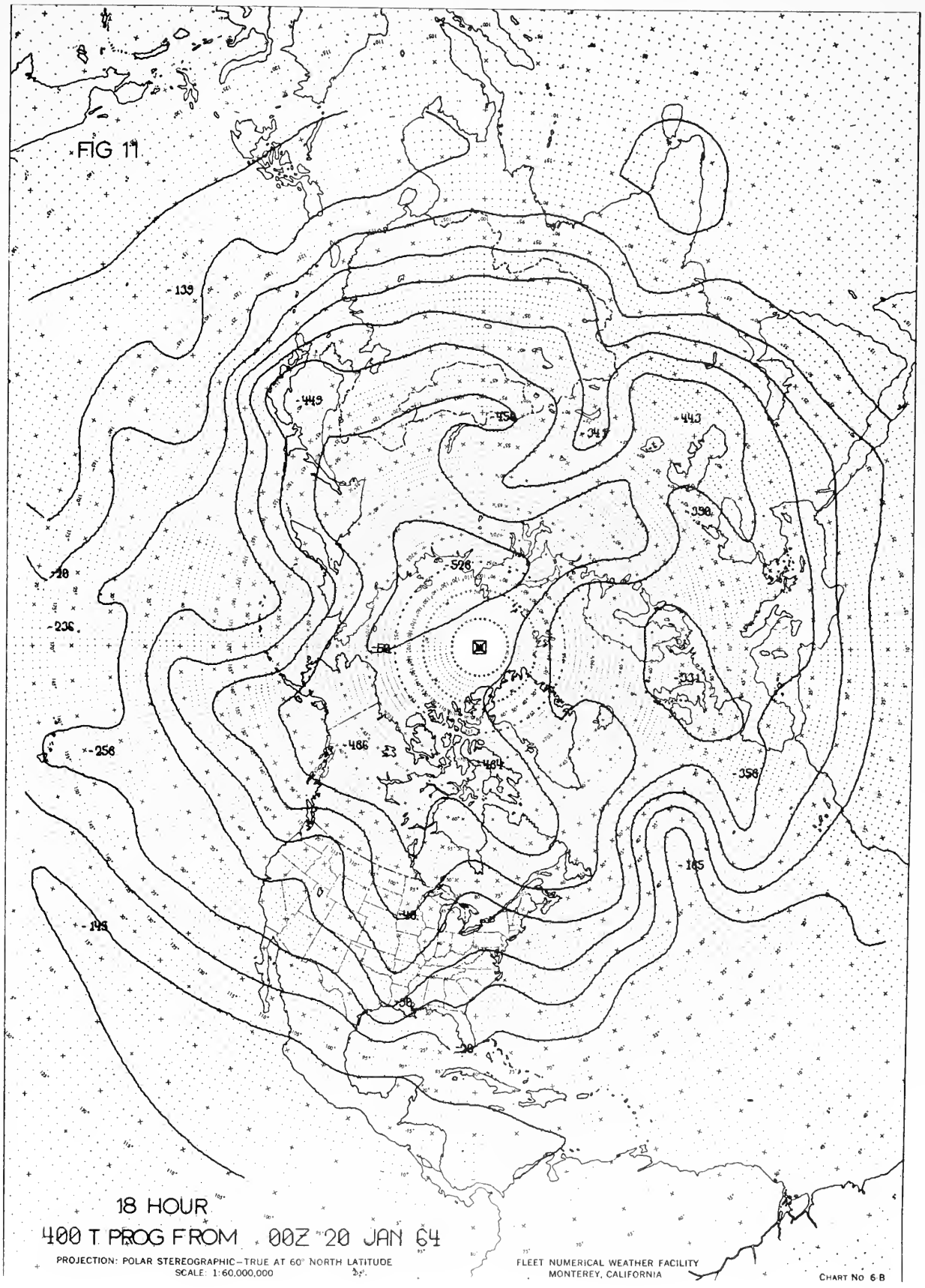
FIG 11
18 HOUR
400 T PROG FROM 00Z 20 JAN 64
PROJECTION: POLAR STEREOGRAPHIC—TRUE AT 60° NORTH LATITUDE
SCALE: 1:60,000,000
FLEET NUMERICAL WEATHER FACILITY
MONTEREY, CALIFORNIA
CHART NO 6-8

thesB3695
Some numerical experiments with the prim
3 2768 002 13700 2
DUDLEY KNOX LIBRARY